Published in final edited form as:
Proteins. 2010 March ; 78(4): 932–949. doi:10.1002/prot.22618.

Symmetry-Restrained Molecular Dynamics Simulations Improve Homology Models of Potassium Channels

Andriy Anishkin[1,*], **Adina L. Milac**[2,3,*], and **H. Robert Guy**[2,†]

[1]Department of Biology, University of Maryland, College Park, Maryland 20742 U.S.A.

[2]Laboratory of Cell Biology, CCR, National Cancer Institute, National Institutes of Health, Bethesda, Maryland 20892-5567 U.S.A.

[3]Institute of Biochemistry of the Romanian Academy, Splaiul Independentei 296, 060031, Bucharest 17, Romania

Abstract

Most crystallized homo-oligomeric ion channels are highly symmetric, which dramatically decreases conformational space and facilitates building homology models (HMs). However, in molecular dynamics (MD) simulations channels deviate from ideal symmetry and accumulate thermal defects, which complicate the refinement of HMs using MD. In this work we evaluate the ability of symmetry constrained MD simulations to improve HMs accuracy, using an approach conceptually similar to CASP competition: build HMs of channels with known structure and evaluate the efficiency of proposed methods in improving HMs accuracy (measured as deviation from experimental structure). Results indicate that unrestrained MD does not improve the accuracy of HMs, instantaneous symmetrization improves accuracy but not stability of HMs during subsequent unrestrained MD, while gradually imposing symmetry constraints improves both accuracy (by 5-50%) and stability of HMs. Moreover, accuracy and stability are strongly correlated, making stability a reliable criterion in predicting the accuracy of new HMs.

Keywords

symmetry annealing; ion channels; structure prediction; structure refinement

Introduction

Transmembrane (TM) proteins are widespread (30% of all genes encode membrane proteins) and form attractive targets for drug design (60% of approved drug targets are membrane proteins (1)). Unfortunately, our understanding of their functional mechanisms is hampered by limited structural information. The number of determined structures for TM proteins is about two orders of magnitude less than for soluble proteins (2). Moreover, functional mechanisms of many membrane proteins involve a series of conformational states, but often the structure of only one state has been determined. Many solved membrane protein structures have prokaryotic origin; whereas, many pharmaceutical targets are human homologues. Therefore theoretical approaches are an essential tool in structural studies of TM proteins. Homology modeling is probably the most reliable method (3) for predicting the structures of new proteins (“target”) based on their sequence similarity with proteins of

† Correspondence to H. Robert Guy, Laboratory of Cell Biology, National Cancer Institute, National Institutes of Health, Bethesda, Maryland 20892-5567 U.S.A. Phone: 301.496.2068; Fax: 301 402 4724, guyh@mail.nih.gov.
*These authors contributed equally to this work

known structure ("template"). The accuracy of the resulting model depends on several factors: a) accuracy of the template; b) the level of sequence identity (above 30% typically yields a model with accuracy comparable to a low resolution crystal structure (3)); c) the accuracy of the target-template sequence alignment (the most important factor); and d) the number of available templates (4). But homology modeling of membrane proteins faces important challenges; e.g., the number of available templates is rather limited and their prokaryotic origin often leads to using distantly-related templates and the amino-acid composition is biased towards hydrophobic residues, which often makes the alignment ambiguous. These factors decrease the accuracy of the resulting models up to the level of a low-resolution crystal structure, with a Root Mean Square Deviation (RMSD) above 3Å, which makes them less useful for drug design purposes or inferring functional properties. Further improvement of template-based structure prediction methods has been modest in recent studies reported at CASP (5), therefore refinement methods in homology modeling need to be improved.

Although molecular dynamics (MD) with either explicit or implicit solvent has been shown to accurately discriminate native from erroneous, non-native structures (6), the method has limited capability for structure refinement of low-resolution models (7,8), and is applicable only to small to medium size proteins. In fact, here we report that unrestrained MD simulations slightly increased the RMSD of HMs of closed channels. A major difficulty with MD refinement might be that the native structure is not the lowest free energy state in simulations (9), although the situation can be significantly improved by optimization of the force field parameters (10,11). Regardless of the precision of the force field, another limitation of MD refinement of molecular models is that typical 10-100 ns computational timescale may not be sufficient to explore vast conformational spaces. For those homo-oligomeric proteins that have a symmetric lowest energy state (12), it is feasible that beneficial advances of individual subunits can be spread and conformational space can be limited by intermittent application of symmetry restraints. Our goal in this project is to assess the ability of symmetry restrained MD simulations to improve HMs accuracy. To this purpose, we used a strategy similar to the CASP competition: we built HMs of channels with experimentally determined structures, applied a simulation protocol, and evaluated the extent to which the method improved HMs accuracy as measured by the deviation from the corresponding crystal structure. The proposed methodology can be applied also to refine the low-resolution experimental structures as well as structures produced in simulations, e.g. steered MD or coarse-grain. We focus our attention on ion channels because they represent an important category of proteins with few known pharmaceutical target structures and because many of the targets are located in a central pore surrounding the axis of rotational symmetry (13,14). Symmetry has been previously incorporated in modeling the structure of ion channels such as Shaker K^+ (15), hERG (16), Kir (17), KcsA (18), KvAP (19), NaChBac (20,21), MscL (22) or MscS (23,24). However, to our knowledge this is the first study that thoroughly evaluates the benefits of incorporating symmetry restraints in MD simulations in the refinement step of structure prediction and that compares different approaches of applying symmetry restraints.

Several explanations have been proffered for why symmetry is a common feature of oligomeric proteins; e.g., symmetry may confer functional advantages since is often associated with cooperativity and allosteric regulation (12,25), symmetric structures may fold more easily (26,27), symmetry may increase structural stability (28-30), and symmetric structures may be more tolerant to mutations (31). Whatever the reason for symmetry, from the modeling perspective, enforcing symmetry restraints significantly reduces the number of degrees of freedom to be explored, making calculations on large systems more tractable and accurate predictions more achievable, as shown by the symmetrization protocol implemented in ROSETTA program (32). As opposed to other protocols incorporating

symmetry, our method has multiple advantages: a) it can be used after the modeling stage, for structure refinement, which makes it applicable to low-resolution experimental structures; b) the protein is embedded in membrane and the system is solvated, using an all-atom representation of both protein and environment, which allows more precise evaluation of atomic interactions; c) the degree of symmetry can be altered, allowing examination of multiple types of symmetry (In this case we used 4-fold symmetry, since the target structures used to evaluate the methods have 4-fold symmetry); d) the symmetry restraints can be turned on and off or applied with the lower strength of the restraints, so that transitions from symmetry to asymmetric states can be studied; and e) symmetry restraints may be selectively applied to a subset of all protein atoms.

Obviously no protein assembly will have perfect symmetry at all times. Thermal fluctuations will cause deviations from symmetry at any instance in time and perturbation from perfect symmetry may be essential in some systems for dynamic functions such as channel gating (33-36), membrane insertion or assembly processes. However understanding dynamic processes is not the goal of our study. On the contrary, our focus is on time-averaged, static, low energy conformations comparable to the experimentally determined crystal structures. Although all the simulations were performed at 303 K to effectively explore the conformational space, by the end of the annealing with gradually increasing symmetry restraints the fluctuating channels have converged into this kind of structure. The high temperature relative to normal crystallographic conditions may account for some of the divergence of the models from the crystal structures during the unrestrained MD simulations.

Methods

Homology modeling and system preparation

Selection of the structures to be used as benchmarks was based on several criteria: 1) the structures should correspond to the same conformational state; 2) the size of the proteins should be small enough to allow sampling of longer timescales during molecular dynamics simulations; 3) the resolution of the structures should be good enough to allow moderately accurate, but low resolution modeling; 4) the sequence identity between homologs should be less than 30%. These criteria were satisfied by four crystal structures of ion channels in closed conformation: K^+ Channel KcsA at 2 Å resolution, pdb code 1k4c (37); NaK channel at 2.4 Å resolution, pdb code 2ahy (38); inwardly rectifying K^+ channel KirBac3.1 at 2.6 Å resolution, pdb code 1×14 (39) and K^+ channel MlotiK at 3.1 Å resolution, pdb code 3beh (40). Although MlotiK is a 6TM channel, we truncated the structure at residue 126 and used only the pore domain, to be consistent with the other structures included in our study.

Three HMs were built for every protein, using each of the remaining three proteins as templates. The sequence alignment used during modeling (Fig. 1 A) corresponds to the structural alignment. Templates consisted of symmetric tetrameric crystal structure and each chain was modeled individually, based on the corresponding chain in the template. All initial models were generated using Modeller 9v1 (41,42). Since the sequence identity level is low (between 15% and 25% in all cases, except between KcsA and MlotiK, for which it is 40%) and the structures differ in some regions by as much as 10 Å (Fig. 1 B and C), the process corresponds to “remote homology modeling” (which is usually the case for transmembrane proteins) and unrefined low resolution models cannot be expected to be precisely accurate. Therefore refinement protocols that improve the accuracy and precision of the models are needed if resulting models are to be useful in structure-based drug design.

The four crystal structures and the twelve HMs (three for each channel) were used as starting structures for MD simulations and were processed according to the following protocol:

a. Hydrogen atoms were added; ionizable residues were in their default protonation state. The only exception is Glu71 in KcsA, which was constructed in a protonated state to form a diacid hydrogen bond with the carboxylate group of Asp80, as shown by previous theoretical studies (43,44).

b. For consistency, the subunits in all the crystal structures and the HMs were renamed A, B, C, and D counting clockwise when viewed from the selectivity filter side. The structures were oriented so that the fourfold rotational symmetry axis coincided with z, with extracellular and selectivity filter side facing the positive direction. The channel was positioned along z coordinate to have the best match of the surface hydrophobicity pattern to the lipid membrane patch.

c. Ions were positioned in the selectivity filters of HMs the same way as in the corresponding target crystal structures and intercalated with two water molecules, since water is essential for ion conduction (45). Ions were not restrained during all the simulations and annealings. In simulations where the selectivity filters of the target and template were similar (like KcsA vs. KirBac models) the ions tended to stay within the filter, (often with exchange of the outmost ion to the one from the bulk by the next simulation/annealing cycle), whereas in the models with significantly different filters (e.g. NaK vs. KirBac) one or two outmost ions usually left the filter within the first few nanoseconds (see section related to selectivity filter under Results). Also the hydrophobic cavity of HMs was solvated with the same number of water molecules as the corresponding target crystal structure. Although the cavity of the HMs is sometimes larger, if extra water is trapped there, the protein would have difficulties in changing conformation to the correct one. The number of water molecules embedded into the pore cavity (25 for KcsA, 38 for KirBac, 4 for MlotiK and 34 for NaK) was estimated based on the bulk water density and the size of the target structure cavity. However during the simulations the number of water molecules in the cavities gradually decreased in most systems, on average down to 77% of the original amount, apparently due to the hydrophobic nature of the cavity-lining side chains that have promoted partial dehydration. Despite the closed conformational state of the channels, water displayed the ability to slowly permeate through the fluctuating gate and (more rarely) between the helices in that region. Over the course of 35 ns simulation (either continuous unrestrained simulation or a set of intermittent 8-ns unrestrained simulations and 1-ns annealings) on average about 74% of the water molecules present in the cavity at the start have left it by the end, whereas some amount of the water molecules from the bulk (~51% of the starting amount) have permeated into the cavity. The exact numbers are provided in Supplementary Table SI. Apparently, the water in the cavities is still far from reaching the dynamic equilibrium, but the continuous two-way exchange between the bulk and the cavities suggests the precise number of the water molecules in the cavities at start is not critical for the output of the symmetry annealings.

d. Channels were embedded into a patch of the lipid bilayer of palmitoyl-oleoyl-phosphatidylcholine (POPC) fully hydrated with TIP3P water molecules (46). The lipid bilayer containing on average 225 molecules of POPC was pre-equilibrated in a solvated flexible simulation cell. The dimensions of the rectangular solvent box were chosen so that the minimum distance from the box boundaries to the protein was 30 Å. In the case of HMs, the number of lipids in the top and bottom layers matched the ones for the target structure. If the target structure is less or more

conical than the homology model, a disbalance of the number of lipids can lead to strong mismatch of the lateral pressures in the monolayers of the model thus making it difficult to find the right shape. Considering the in-plane area of the target channels at the levels of the glycerol backbone, the number of lipids included into the upper/lower monolayers were 104/116, 104/125, 104/116, and 104/118 for MlotiK, KcsA, KirBac, and NaK models respectively. The simulation cell area was set at 95×95 $Å^2$ for all the systems, thus leaving ~ 40-60 Å (about 5-7 layers of lipid) between the copies of the channel in the periodic cells. To facilitate conformational rearrangements of channels in the membrane, the system was simulated with an anisotropic flexible cell maintaining 1 bar pressure in z direction and membrane tension of 40 dyne/cm in x-y plane (fixed x to y sizes ratio). Relatively high value of the tension was necessary to maintain an equilibrium area per POPC lipid matching the experimentally measured value of 68.3 $Å^2$ (47,48).

e. K^+ (for MlotiK, KcsA and KirBac) or Na^+ (for NaK) and Cl^- ions were added in order to maintain electroneutrality. One Ca^{2+} ion was placed near the external entrance of the selectivity filter for NaK models in the location suggested by the crystal coordinates.

A sample simulation cell is shown in Fig. 1 D. Structure file was generated using the psfgen plugin in VMD (49). The systems contained the same total number of water molecules, lipids and ions in all the models of the same channel (Supplementary Table SII).

Unrestrained MD simulations

All MD simulations were performed in the NPT ensemble using NAMD2 package (50) developed by the Theoretical and Computational Biophysics Group in the Beckman Institute for Advanced Science and Technology at the University of Illinois at Urbana-Champaign, with the CHARMM27 force field parameters (51) including the grid-based CMAP correction (52) for the φ-, ψ-angular dependence of the energy. This is especially important for α-helical proteins (as the systems simulated in this work), since CMAP not only yields significant improvements in the distribution of dihedral angles, but also corrects the tendency of CHARMM force field to distort α-helix structures to π-helix structures (53,54).

The simulation systems were subject to a stepwise equilibration before the production phase, involving initial 1000 steps of energy minimization, followed by 100 ps of gradual heating to 303 K with the protein constrained to the initial coordinates, and 4ns of simulation in which protein backbone was constrained but lipids were allowed to pack around the protein.

After the initial minimization, heating, and equilibration stages, the production phase of each MD unrestrained simulation used a time step of 1 fs for the bonded interactions, with coordinates saved every 1 ps. The Langevin piston method (55,56) was used to maintain a constant pressure of 1 atm. The temperature, set to 303 K, was controlled by using Langevin dynamics with a coupling coefficient of 1 ps^{-1}. We used periodic boundary conditions and the particle mesh Ewald method (57) with a real-space cutoff distance of 12 Å and a grid width of 0.97 Å. The switching distance for nonbonded electrostatics and van der Waals interactions was 10 Å and the integration time step was 4 and 2 fs respectively.

Instantaneous Symmetrization

Instantaneous 4-fold symmetric average positions were calculated for all the protein atoms based on the coordinates at the end of the preceding unrestrained cycle. This calculation involved rotating subunits B, C, and D around the pore symmetry axis by 90°, 180°, and 270° respectively (counterclockwise when looking from the selectivity filter side), calculating spatial average positions and assigning these to all the subunits, and then rotating

the subunits back. Conformational conflicts were relaxed in 500 steps of conjugate gradient minimization.

Symmetry-driven simulated annealing (Fig. 2)

During the annealing stages all the protein atoms were gradually driven towards the frequently (every 1 ps) updated 4-fold symmetric average positions using harmonic restraints with spring constant slowly increasing from 0.001 to 10 kcal/mol/Å^2. The rest of the system (lipids, water, and ions) was unrestrained. During the unrestrained simulation stages all medium and protein atoms were free to move.

The value of the spring constant was adjusted (increased or decreased by 10%) every 1 ps to provide the linear decrease in the RMSD (Supplementary Fig. S1). This requirement resulted in nearly exponential growth of the spring constant. A 0.5 Å decrease RMSD from the symmetric average requires about tenfold increase in the spring constant. An average strengthening rate of the constant over the whole annealing stage was about 1%/ps. When RMSD decreases below ~0.3 Å, the adaptive increase in the spring constant required to maintain linear decrease in RMSD is faster, possibly because at this level of restraint the deviation is caused mostly by thermal oscillations of the atoms on the covalent bonds rather than rotational rearrangements around the bonds. The maximum value for the spring constant was set at 10 kcal/mol/Å^2 (above that the simulation becomes unstable causing NAMD2 software to abort the calculations). The symmetry-driven simulated annealing protocol was implemented completely using Tcl scripting abilities of NAMD2 software (50). A sample scripted configuration file for NAMD is provided in the supplement.

Simulation protocol

All systems were subject to successive steps of 8 ns of unrestrained MD simulations followed by 1ns symmetry annealing, as described in Fig. 3. We evaluated the effect of symmetry annealing when applied earlier (after 8ns unrestrained simulation) or later (after 16 ns). We also tested the effect of repeated steps of symmetry annealing, the systems being subject to 3 successive cycles of relaxation/annealing. The results of annealing were backed-up by comparison with structures subject to fully unrestrained simulation.

Data analysis

The size and shape of channels pore was estimated using the program HOLE (58).

Protein secondary structure was estimated using the STRIDE algorithm (59) embedded in VMD (49) (http://www.ks.uiuc.edu/Research/vmd). RMSD relative to the starting structure, target RMSD structure, and the symmetric average was calculated using custom-written Tcl scripts in VMD (49).

Results and Discussion

Accuracy of initial HMs

The most similar proteins (in terms of sequence identity and structural deviation) are MlotiK and KcsA (Fig. 1 B inset), therefore models involving only these two channels are accurate, with less than 3 Å deviation. Since the level of sequence identity between the channels is less than 25% in all other cases (Fig. 1 B inset), the resulting HMs deviate substantially from the correct structure. The most distant is KirBac (15% sequence identity), therefore models in which KirBac is either the target or the template are the least accurate (RMSD ~4 Å relative to the crystal structure). The region with highest deviation is TM1, since its tilt relative to those of KcsA and NaK is slightly different in MlotiK and substantially different in KirBac (Fig. 1 B and C). NaK is most distant for the channel pore and selectivity filter,

because it has a different ion selectivity. Although models involving only KcsA and NaK structures are overall more accurate (RMSD ~3 Å), they contain significant errors in the outer portion of the selectivity filter region. We did not attempt to refine specific regions of a given model by using information from the most closely related homolog for that region, since our goal is not homology modeling *per se*, but testing the ability of symmetry restrained simulations to improve the accuracy of HMs when only one template structure is available. The error level in our models is representative for the modeling of ion channels in general, since usually single templates are available and the sequence identity is below 30%.

Simulations do not alter truncated crystal structures substantially

Effects of the various simulations on the truncated crystal structures are illustrated in the first column of Fig. 4. The RMSD from the original structures during unrestrained simulations remained ≤ 1.2 Å throughout the last half of the simulations for all structures except KirBac, which increased steadily to ~1.7 Å at 35ns. The stability of these structures suggests that the crystal structures are in fact relatively stable when embedded in a lipid bilayer, that (with the possible exception of KirBac) they are not destabilized by the absence of cytoplasmic N- and C-termini domains (and S1-S4 domain for MlotiK), and that the simulation procedures do not alter the structures substantially. The symmetry annealing process reduced the RMSDs; e.g., the values at the end of the second step were ~ 0.7 Å for all structures. These values set the limit of accuracy which can be achieved by using symmetry annealing procedure to refine HMs.

Unrestrained MD simulations do not improve the accuracy of HMs

An initial question we addressed was whether conventional unrestrained MD improves the accuracy of HMs, measured by the RMSD relative to the corresponding crystal structure. As expected, the HMs were noticeably less stable relative to the starting models than were the crystal structures with the average RMSD increase of 3 Å over 35 ns (explicit plots presented in the Supplementary Fig. S2). When compared to the crystal target structure rather than to the starting conformation (black traces in Fig. 4, center and right panels), all twelve HMs displayed high RMSD from the very beginning (3.5 Å on average). None of the models approached target structures in a sustained manner in any of the unrestrained simulations; rather there was actually a small average net increase in the RMSD of 0.5 Å over 35 ns. The only possible exception may be the MlotiK_NaK model, undergoing a decrease in the RMSD of ~0.5 Å during the unrestrained simulation.

Symmetry annealing improves accuracy of HMs more than instantaneous symmetrization

We have compared two ways to apply symmetry restraints to the structure – one is instantaneous assignment of the 4-fold symmetric average conformation (followed by energy minimization to resolve steric conflicts) while another is slow simulated annealing with gradually strengthened harmonic restraints towards constantly updated symmetric conformation (“symmetry annealing”).

To estimate the effect of symmetrization on the accuracy of HMs, we calculated the RMSD of against the corresponding crystal structure, for each trajectory (Fig. 4 for the Cα trace and Supplementary Fig. S3 for the heavy atoms, central and right panels). Even simple instantaneous symmetrization after 8 ns of unrestrained simulation benefits HMs, the RMSD from the “correct” target crystal structure was decreased substantially (21-40%) relative to the RMSD of the original models in four models (KcsA_MlotiK, NaK_MlotiK, KirBac_MlotiK, and MlotiK_NaK), moderately (11-14 %) in four models (MlotiK_KcsA, NaK_KcsA, KirBac_NaK and MlotiK_KirBac) and negligibly (-1-4%) in the remaining four models (see Table I). On the other hand, symmetry annealing is more effective in reducing the RMSD against correct target (Table I). Moreover, when symmetry restraints were

removed, the models obtained with symmetry annealing remained more stable than those obtained with instantaneous symmetrization (gray trajectories in Fig. 4). The 1st step of annealing, applied after 8 ns of unrestrained simulation (pink trajectories in Fig. 4) is more effective than subsequent steps, with an average of 20% of RMSD decrease (most improved is MlotiK_NaK, with 40% decrease of RMSD and least improved is NaK_MlotiK, with 4% decrease in RMSD). On average, the 2nd symmetry annealing step (red trajectories in Fig. 4) was less effective in improving the accuracy of HMs, with less than 10% decrease in RMSD relative to the 1st step. However, the reduction of RMSD relative to the original model was still improved by the 2nd annealing process (average reduction of 1st was 17.3% and 2nd was 22.7%). Eight models improved over the 1st step and the improvement was substantial (> 22%) in 3/12 cases (KcsA_MlotiK, MlotiK_NaK and KirBac_NaK). In contrast, the 3rd annealing step (orange trace) did not alter RMSD values of the models substantially (3/12 models were slightly improved by 0.6-6.3% while 9/12 became slightly worse (0.2-14.6%), see HM values in Table I). Comparing to the non-symmetric conformation right before the annealing, nearly all the structures improved during the 3rd symmetrization. Therefore the predominant reason for decrease in the quality of the models might be the drift away from the target during the preceding third cycle of unrestrained rather than the 3rd annealing *per se*. Apparently, after two previous (generally successful) rounds of refinement the structures have on average approached the target enough so that the chances to find further improvement by some of the subunits are exceeded by the chances to deviate away from the target due to the thermal fluctuations.

By comparing the starting models to those at the end of the 2nd symmetry annealing process (red trajectory), one can classify the models into four categories: A) highly improved models, with > 40% decrease of RMSD against “correct” crystal structure (KcsA_MlotiK, MlotiK_KcsA, and MlotiK_NaK); B) substantially improved models with improvements of 29-32% (NaK_KcsA and KirBac_NaK); C) slightly improved models with improvements of 7-14% (NaK_MlotiK, KirBac_MlotiK, KirBac_KcsA, NaK_KirBac and KcsA_KirBac), and unimproved models (KcsA_NaK and MlotiK_KirBac). The improvement is even more marked when RMSD values at the end of the 2nd annealing step are compared to those at the end of the 35 ns unrestrained simulations (Fig. 4).

HMs improved least by symmetry annealing were those involving KirBac (see last row and column in Fig. 4). It is unclear whether the failure in most cases of the symmetry annealing process to improve these model is due to the greater evolutionary distance, the greater tilt in the TM1 helices, or the greater instability of the truncated KirBac crystal structure during unrestrained MD simulations, which may be due to missing N- and C-termini domains.

Although symmetry annealing markedly improves only some of the original homology models, the improvement by symmetrization is more widespread if compared to the non-symmetrized structure before the beginning of the annealing (see Fig. 4 and Table I). This trend may be related to deviations during unrestrained MD simulations rather than flaws in initial homology modeling. The ability of the symmetry annealing to repair some of the simulation-caused defects can be useful for refinement of the structures that were derived or significantly transformed by simulation since extreme conditions (steering forces, high voltages, membrane stretch) are often used to cause the required conformational changes within the simulational timescale. For example, models of open conformations of mechanosensitive channels have been developed by stretching structures of closed states during MD simulations; however, this stretching process also tends to damage the structure (60).

Since the target crystal structures are perfectly symmetric, one may argue that the decrease in RMSD (improvement in model accuracy) may simply be an artifact due to comparison

with a symmetric structure (although when the simulations were just started, the initial HMs had symmetric backbone conformations but still displayed substantial deviation from the target). To test this "artifact" hypothesis, we calculated the RMSD against the crystal structure for each chain separately (for that, each chain was aligned with the corresponding fragment of the target independent of the rest of the channel. See Supplementary Fig. S4). Results show that substantial improvement occurs for the majority of subunits independent of the symmetric relationship among the subunits; i.e., each chain structure gets somewhat closer to the correct target and the overall effect is additive. Since the annealed structure is symmetric, the variation in the degree of improvement among individual subunits of a channel is dictated by the different starting deviations of the subunits from the target before the annealing. That variation, acquired during the unrestrained simulation might be largely caused by the strong and heterogeneous influences of the surrounding lipid bilayer that is prone to spontaneous multi-nanosecond undulations and thickness fluctuations (61) with lateral tension and pressure forces on the scale of the hundreds of bar (62). Typically, the subunits that were further away from the target acquire more improvement on symmetrization, while those that were closer improve less, although favor the improvements of the other subunits by serving as "anchors" that have found more stable conformation and pull others towards it through symmetry restraints (e.g. see NaK_KcsA model improvement during the first annealing on the Supplementary Fig. S4).

Effect of symmetry constraints on protein core

Since the pore region is most important from the pharmacological point of view, we were interested in the effects symmetry constraints have on the shape of the pore and especially the cavity below the selectivity filter, which constitutes a major drug binding region (DBR). To understand the general effect symmetry annealing has on the central region, we calculated the RMSD of the 'core' P through TM2 segment (Fig. 5). The results indicate a similar trend as the RMSD for the whole structures, but the absolute values of deviations from the target were lower, as expected. RMSDs from the target at the end of the 2nd annealing were less than or equal to 1 Å for 7/12 models (KcsA_MlotiK, KirBac_MlotiK, MlotiK_KcsA, NaK_KcsA, KirBac_KcsA, MlotiK_NaK, and MlotiK_KirBac), these RMSD values being about the same as those of the target crystal structures, and were less than or equal to 2.3 Å the remaining models. The symmetry annealing process produced no significant improvement relative to initial HMs for the six models involving KirBac (last row and column in Fig. 5); three of these actually got worse during the simulations and the improvements for the other four were small (Table II). Symmetry annealing did improve the core region relative to the initial HMs of the remaining six models substantially (46-60% for KcsA_MlotiK, MlotiK_KcsA, NaK_KcsA, and MlotiK_NaK; 16-22% for KcsA_NaK and NaK_MlotiK in Table II). These improvements in modeling the core could be important for structure-based drug design, since errors in modeling the TM1 and 'turret' segment linking TM1 to P contribute to much of the deviation for the complete models, but do not contribute errors to many drug binding sites. It is interesting to note that HMs described as less accurate based on whole structure RMSD (KirBac_KcsA, KcsA_KirBac, KirBac_MlotiK and MlotiK_KirBac) are very accurate in the core region, with RMSD values almost equal to the corresponding crystal structures. This implies that errors in these structures originate mainly in the differences between TM1 segments, which in KirBac and MlotiK structures have an exceptionally pronounced tilting, giving rise to errors in the HMs when KirBac or MlotiK are either the target or the template.

Symmetry annealing improves the shape of the drug binding region

Although the previously calculated core RMSD (Fig. 5) gives a good estimate of structure accuracy, it does not reveal details on the size and most importantly shape of the DBR. Therefore we compared the HMs with the crystal structures, both before simulation and after

the second step of symmetry annealing, in terms of pore shape and diameter (Fig. 6). While for MlotiK, KcsA and KirBac crystal structures the pore shape remains practically unchanged, in the case of NaK the pore slightly constricts (~0.2 Å decrease in radius, in the DBR). For the HMs, in all cases the shape of the DBR became more similar to the corresponding region in the crystal structure. The shape of DBR can be classified into two categories: a large central cavity of ~4.5 Å in radius (as is the case of KcsA and NaK) or three small cavities of ~2 Å in radius (as is the case of MlotiK and KirBac). As a consequence, models involving structures in the same category (e.g. KcsA_Nak and NaK_KcsA or KirBac_MlotiK and MlotiK_KirBac) are most accurate in the DBR, while HMs involving structures in different categories display an initial incorrect shape of DBR. Symmetry annealing always improves the DBR. The most significant changes occur in KcsA_MlotiK, NaK_MlotiK and KcsA_KirBac case, where the shape of the initial HMs had a central blob but the symmetricized model is virtually identical in shape and size to the target crystal structure.

Symmetry annealing effect on the orientation (tilt) of transmembrane segments in HMs

To estimate the effect of symmetry annealing on different regions of the channels and better understand the contribution of each region to the overall HMs accuracy, we compared the HMs before simulation and most improved HMs after annealing with the corresponding crystal structure. Since previous RMSD analysis (Fig. 4) indicated that in most cases the maximum improvement occurs at the end of second annealing step, we chose these structures for comparison (Fig. 7). Results indicate that symmetry annealing improved the orientation of both TM segments in MlotiK and KcsA models regardless of the template that has been used, did not significantly affect the TM segments of KirBac models and improved only TM2 segment of NaK models.

Symmetry annealing produces mixed results for the selectivity filter

The ion selectivity of these channels is determined by the P segment. The greatest differences among the crystal structure P segments occurs when NaK, which is permeant to both Na^+ and K^+, is compared to MlotiK, KcsA or KirBac, which are selective for K^+.

Consequently, improvements in the P segment occur only in the models involving K-selective channels, where target-template differences are small enough to be overcome. In the other cases, where NaK is either the target or the template, models still retain substantial errors, especially in the outer entrance formed by the C-terminus of the P segment (Fig. 7). However, the errors in the selectivity filter might be generated by the fact that during simulations ions escaped from the selectivity filter, which significantly affected interactions maintaining the integrity of this region (Supplementary Fig. S5).

Symmetry annealing improves protein stability

To evaluate the effect of symmetrization on protein stability, we calculated the RMSD of Cα trace during each trajectory, using as reference the structure at the beginning of each step (Fig. 8). While instantaneous symmetrization makes the structure even less stable than unrestrained symmetrization (grey lines), each step of symmetry annealing always improves stability.

Note that structure stability correlates very well with improvement in structure accuracy (Supplementary Fig. S6). The most stable models (MlotiK_KcsA, NaK_KcsA, KcsA_MlotiK, MlotiK_NaK and KirBac_NaK), with less than 1 Å deviation of the Cα trace during the 8 ns simulation following symmetry annealing, are also the most improved ones, with 50% decrease in RMSD against crystal structure. In contrast, the remaining models, with a modest improvement during symmetry annealing, show a deviation of more than 1 Å.

Thus, results of unrestrained MD simulations following symmetry annealing can be useful in evaluating the likelihood that the symmetry annealing process improved the models.

Longer unrestrained simulation time does not increase effectiveness of subsequent symmetry annealing

To test whether allowing the protein to drift farther away from the initial structure would improve the results of symmetry annealing by a more efficient sampling of the conformational space or on the contrary, whether a structure that deviates more from the starting models is more difficult to improve, we applied symmetry annealing after 16 ns of unrestrained simulation (Supplementary Fig. S7, violet lines), followed by 8ns unrestrained simulation (Supplementary Fig. S7, teal lines). The results indicate that the annealing is more (five models) or equally effective when applied earlier, at 8 ns.

RMSF values are not affected substantially by symmetry annealing and do not correlate with model accuracy

We also calculated the fluctuation of each residue position relative to its average position (RMSF values) during the last 8 ns of unrestrained and post symmetrized simulations. All values were less than 2.5 Å and were not substantially different between unrestrained simulations and simulations following symmetrization. We also observed no substantial correlation between the accuracy of the models (deviation values in Fig. 7) and the RMSF values.

Symmetry annealing corrects the thermal defects in protein structure (Fig. 9)

The analysis presented thus far have been limited to spatial rearrangements or slight bending of homologous domains with preserved secondary structures because the secondary structure pattern is nearly identical for all the crystal templates. To test the ability of symmetry annealing to improve quality of the secondary structure pattern as well, we first distorted the KcsA channel by simulations at high temperature (600K) for 8 ns with CMAP correction. However the amount of the thermal defects was deemed too small, so the CMAP correction in the force field was removed to increase the rate of defects accumulation and the simulations were continued for 8 more ns. The STRIDE algorithm embedded in VMD was used to quantify effects of these simulations on the secondary structure. The net number of residues in the transmembrane regions (residues 24-51 and 86-116) satisfying the criteria for alpha-helical structure was taken as a rough measure. Helicity decreased by 32% on heating without CMAP.

Next the ability of three types of simulation procedures to restore the structure were examined:

1. unrestrained 8 ns simulation of the damaged structure at 303.15 K and with CMAP on,
2. annealing at 600 K and without CMAP - the same conditions as was the damage done
3. symmetry annealing procedure at normal temperature (303.15 K), with CMAP correction on, as described in the Methods section.

The first procedure produced only slight improvement; the helicity increased form 68% to only 78% of the original value. After 4 ns most of the defects are still there, including the major kink in TM1 helix and the double kink in TM2 helix. The uncoiled few turns at the ends of many helices are still uncoiled. The selectivity filter became even worse after the unrestrained simulation. The second procedure increased helicity form 68% to 83% of the original value helicity. The third procedure was the most regenerative (see Fig. 9 for visual

comparisons of original, perturbed, and restored structures). Helicity increased to 87% of the original value (56% of the thermal defects were 'healed'). Visual inspection reveals critical distinction of the healing by symmetrization comparing to only CMAP correction: while both approaches partially restore the uncoiled residues at the ends of the alpha-helical regions, symmetry annealing much more effectively removes the kinks in the middle of the transmembrane helices which are able to alter dramatically the overall structure. To illustrate this fact, the content of the helical region only in the transmembrane helices was estimated with the first and last turns excluded from consideration. With that criterion, about one fifth of the residues are damaged by heating, simulation with CMAP correction at 303.15 K restores 63% of them, the annealing at 600 K without the correction restores 89%, while annealing at 303.15K with CMAP restores 100% of the helicity defects. MD simulations typically introduce substantial errors at untethered beginning and ends of structurally incomplete models when segments that precede and follow the modeled region are missing. It would thus be prudent in actual homology modeling to restrain secondary structures of these loose ends to conform to those of the template if substantial divergence occurs in the absence of restraints.

To measure the deviation of the overall helix shape from the original crystal structure, each of 8 transmembrane helices of KcsA in the damaged and 'healed' structures was independently aligned with the original fragment. The estimated RMSD for alpha-carbons (3.23 Å) was decreased by 5%, 36%, and 41% by procedures 1, 2, and 3 respectively.

Conclusions

In this work we evaluated different protocols for incorporating symmetry constraints in the refinement of HMs with the purpose of increasing the accuracy of predicted structures. Our analysis of conventional and symmetry-restrained MD simulations of the crystal structures and homology models of potassium channels suggest several conclusions:

1. Unrestrained simulation does not improve the HMs in the observed timescale, but can be useful in perturbing structures to escape local minima and in evaluating stabilities of models.
2. Two cycles of unrestrained MD and symmetry annealing improved 10/12 of the models, and improvement was substantial in five cases. Maximum benefit was achieved at the 2nd annealing step; the 3rd step made models slightly worse.
3. The annealed models have improved stability, which correlates with the progress of the refinement. For new (unknown) targets, stability might be used as a rough measure of success.
4. Symmetry annealing is more effective in improving HMs accuracy than instantaneous symmetric averaging and produces more stable structures.
5. Excessive prolongation of unrestrained simulations does not improve results of symmetry annealing; e.g., the annealing was actually more effective after 8ns unrestrained simulations than after 16ns.
6. Symmetry annealing is effective in 'healing' thermal defects accumulated during unrestrained simulations.

Due to its conceptual simplicity, symmetry-driven simulated annealing is compatible with all the major force fields and MD software, and can be useful for simulation-based structure refinement as well as in searching for new conformational states under biasing conditions. While this study demonstrates the utility of the symmetry annealing method, it was not designed to optimize the method or to determine which factors are more important.

Improvements by symmetry annealing may be due to two effects: on one hand, averaging of simulation-induced effects on multiple identical subunits or following multiple simulations of a single subunit may help identify the more stable conformations even in the absence of symmetry; on the other hand, interactions among identical subunits is more restricted when required to be symmetric (as used in Rosetta). The study presented here does not attempt to identify which of these is more important. The effectiveness of the refinement procedure almost certainly can be further improved by optimization of the time between symmetry annealing steps, temperature and other conditions during unrestrained simulations and annealing stages. The models might be improved by combining in the averaging steps results from multiple simulations or obtained using multiple templates. When original structures for several evolutionary homologues are available, combining results from multiple templates with emphasis of using templates regions where sequences and functional mechanisms are more similar (e.g., the NaK_KcsA model could have been improved if the selectivity filter from KirBac had been used as the template; or possibly both the NaK_KcsA and KirBac_KcsA models could have been improved if symmetry restraints were used to pull these models into a single model). Application of additional restraints, e.g. to retain the ions in remote models of the selectivity filter or restraining ‘loose ends’ to retain secondary structures of templates might prevent damage of these regions in models. Also, we have not yet compared results obtained with the annealing procedure to those obtained when symmetry restraints are imposed throughout the MD simulations of HMs.

Our finding that unrestrained MD simulations do not improve HMs relative to target crystal structures does not denigrate the importance of MD. Crystal structures are time-averaged static representations that attempt to identify a unique location where each atom is most likely to be in stable conformational states, which to a certain degree is approximated by the simulated coordinates when averaged over a long period of time. MD is an invaluable tool in analyzing the dynamics of how atomic positions may deviate from these locations at any instance in time and in analyzing dynamic processes such as ion permeation and gating. The symmetry annealing procedure described here is intended to mimic the crystal-based models, and can be used in conjunction with unrestrained simulations to analyze more dynamic processes. Advantage of the method are that the restraints can be turned on and off, the strengths of the restraints can be adjusted, the restraints can be applied to only selected residues or atoms, and the degree of symmetry can be adjusted; e.g., the channel models could be restrained to only two-fold instead of four-fold symmetry.

Homology modeling of distantly related K^+ channels is limited by the fact that N- and C-termini domains that precede TM1 and follow TM2 often have no homology and cannot be included in the models. If these domains affect positions of TM domains substantially, then all homology modeling refinement procedures are likely to fail. It may be possible to detect this type of effect by MD simulations of the truncated crystal structures; e.g., the inability of symmetry annealing to improve models involving KirBac may be related to the fact that the truncated KirBac crystal structure is less stable during long unrestrained MD simulations.

In summary, we have shown that symmetry restraints improve homology models of ion channels, and we are optimistic that homology models of symmetric channels can be developed that are sufficiently accurate and precise for structure-based drug design, even when only distantly related template structure are available.

Supplementary Material

Refer to Web version on PubMed Central for supplementary material.

Acknowledgments

This study utilized the high-performance computational capabilities of the Biowulf Linux cluster at the National Institutes of Health (NIH), Bethesda, MD. This work was supported by the Intramural Research Program of the NIH, National Cancer Institute, Center for Cancer Research. The authors thank Drs. Stewart Durell, Yinon Shafrir, Sijung Yun (LCB, NCI) and Sergei Sukharev (UMCP) for fruitful discussions.

References

1. Yildirim MA, Goh KI, Cusick ME, Barabási AL, Vidal M. Drug-target network. Nat Biotechnol. 2007; 25(10):1119–1126. [PubMed: 17921997]
2. Jayasinghe S, Hristova K, White SH. MPtopo: A database of membrane protein topology. Protein Sci. 2001; 10(2):455–458. [PubMed: 11266632]
3. Xiang Z. Advances in homology protein structure modeling. Curr Protein Pept Sci. 2006; 7(3):217–227. [PubMed: 16787261]
4. Ginalski K. Comparative modeling for protein structure prediction. Curr Opin Struct Biol. 2006; 16(2):172–177. [PubMed: 16510277]
5. Kryshtafovych A, Venclovas C, Fidelis K, Moult J. Progress over the first decade of CASP experiments. Proteins. 2005; 61 7:225–236. [PubMed: 16187365]
6. Taly JF, Marin A, Gibrat JF. Can molecular dynamics simulations help in discriminating correct from erroneous protein 3D models? BMC Bioinformatics. 2008; 9:6. [PubMed: 18179702]
7. Fan H, Mark AE. Refinement of homology-based protein structures by molecular dynamics simulation techniques. Protein Sci. 2004; 13(1):211–220. [PubMed: 14691236]
8. Chen J, Brooks CL 3rd. Can molecular dynamics simulations provide high-resolution refinement of protein structure? Proteins. 2007; 67(4):922–930. [PubMed: 17373704]
9. Wroblewska L, Skolnick J. Can a physics-based, all-atom potential find a protein's native structure among misfolded structures? I. Large scale AMBER benchmarking. Journal of Computational Chemistry. 2007; 28(12):2059–2066. [PubMed: 17407093]
10. Jagielska A, Wroblewska L, Skolnick J. Protein model refinement using an optimized physics-based all-atom force field. PNAS. 2008; 105(24):8268–8273. [PubMed: 18550813]
11. Wroblewska L, Jagielska A, Skolnick J. Development of a Physics-Based Force Field for the Scoring and Refinement of Protein Models. Biophys J. 2008; 94(8):3227–3240. [PubMed: 18178653]
12. Goodsell DS, Olson AJ. Structural symmetry and protein function. Annu Rev Biophys Biomol Struct. 2000; 29:105–153. [PubMed: 10940245]
13. Zimmerman AL. Two B or not two B? Questioning the rotational symmetry of tetrameric ion channels. Neuron. 2002; 36(6):997–999. [PubMed: 12495616]
14. Silberberg SD, Swartz KJ. Structural biology: Trimeric ion-channel design. Nature. 2009; 460(7255):580–1. [PubMed: 19641581]
15. Durell SR, Shrivastava IH, Guy HR. Models of the structure and voltage-gating mechanism of the Shaker K^+ channel. Biophys J. 2004; 87(4):2116–2130. [PubMed: 15454416]
16. Tseng GN, Sonawane KD, Korolkova YV, Zhang M, Liu J, Grishin EV, Guy HR. Probing the outer mouth structure of the HERG channel with peptide toxin footprinting and molecular modeling. Biophys J. 2007; 92(10):3524–3540. [PubMed: 17293393]
17. Guy HR, Durell SR. Structural models of Na^+, Ca^{2+}, and K^+ channels. Soc Gen Physiol Ser. 1995; 50:1–16. [PubMed: 7676315]
18. Durell SR, Hao Y, Guy HR. Structural models of the transmembrane region of voltage-gated and other K^+ channels in open, closed, and inactivated conformations. J Struct Biol. 1998; 121(2):263–284. [PubMed: 9615442]
19. Shrivastava IH, Durell SR, Guy HR. A model of voltage gating developed using the KvAP channel crystal structure. Biophys J. 2004; 87(4):2255–2270. [PubMed: 15454428]
20. Shafrir Y, Durell SR, Guy HR. Models of the structure and gating mechanisms of the pore domain of the NaChBac ion channel. Biophys J. 2008; 95(8):3650–3662. [PubMed: 18641075]

21. Shafrir Y, Durell SR, Guy HR. Models of voltage-dependent conformational changes in NaChBac channels. Biophys J. 2008; 95(8):3663–3676. [PubMed: 18641074]
22. Sukharev S, Durell SR, Guy HR. Structural models of the MscL gating mechanism. Biophys J. 2001; 81(2):917–936. [PubMed: 11463635]
23. Anishkin A, Akitake B, Sukharev S. Characterization of the resting MscS: modeling and analysis of the closed bacterial mechanosensitive channel of small conductance. Biophys J. 2008; 94(4): 1252–1266. [PubMed: 17981908]
24. Anishkin A, Kamaraju K, Sukharev S. Mechanosensitive channel MscS in the open state: modeling of the transition, explicit simulations, and experimental measurements of conductance. J Gen Physiol. 2008; 132(1):67–83. [PubMed: 18591417]
25. Blundell TL, Srinivasan N. Symmetry, stability, and dynamics of multidomain and multicomponent protein systems. Proc Natl Acad Sci U S A. 1996; 93(25):14243–14248. [PubMed: 8962033]
26. Frauenfelder H, Sligar SG, Wolynes PG. The energy landscapes and motions of proteins. Science. 1991; 254(5038):1598–1603. [PubMed: 1749933]
27. Nymeyer H, García AE, Onuchic JN. Folding funnels and frustration in off-lattice minimalist protein landscapes. Proc Natl Acad Sci U S A. 1998; 95(11):5921–5928. [PubMed: 9600893]
28. Wolynes PG. Symmetry and the energy landscapes of biomolecules. Proc Natl Acad Sci U S A. 1996; 93(25):14249–14255. [PubMed: 8962034]
29. Hoang TX, Trovato A, Seno F, Banavar JR, Maritan A. Geometry and symmetry presculpt the free-energy landscape of proteins. Proc Natl Acad Sci U S A. 2004; 101(21):7960–7964. [PubMed: 15148372]
30. André I, Strauss CE, Kaplan DB, Bradley P, Baker D. Emergence of symmetry in homooligomeric biological assemblies. Proc Natl Acad Sci U S A. 2008; 105(42):16148–16152. [PubMed: 18849473]
31. Choi S, Jeon J, Yang JS, Kim S. Common occurrence of internal repeat symmetry in membrane proteins. Proteins. 2008; 71(1):68–80. [PubMed: 17932930]
32. André I, Bradley P, Wang C, Baker D. Prediction of the structure of symmetrical protein assemblies. Proc Natl Acad Sci U S A. 2007; 104(45):17656–17661. [PubMed: 17978193]
33. Levy Y, Cho SS, Shen T, Onuchic JN, Wolynes PG. Symmetry and frustration in protein energy landscapes: a near degeneracy resolves the Rop dimer-folding mystery. Proc Natl Acad Sci U S A. 2005; 102(7):2373–2378. [PubMed: 15701699]
34. Haider S, Grottesi A, Hall BA, Ashcroft FM, Sansom MS. Conformational dynamics of the ligand-binding domain of inward rectifier K channels as revealed by molecular dynamics simulations: toward an understanding of Kir channel gating. Biophys J. 2005; 88(5):3310–20. [PubMed: 15749783]
35. Jarosławski S, Zadek B, Ashcroft F, Vénien-Bryan C, Scheuring S. Direct visualization of KirBac3.1 potassium channel gating by atomic force microscopy. J Mol Biol. 2007; 374(2):500–505. [PubMed: 17936299]
36. Proks P, Ashcroft FM. Modeling K(ATP) channel gating and its regulation. Prog Biophys Mol Biol. 2009; 99(1):7–19. [PubMed: 18983870]
37. Zhou Y, Morais-Cabral JH, Kaufman A, MacKinnon R. Chemistry of ion coordination and hydration revealed by a K^+ channel-Fab complex at 2.0Å resolution. Nature. 2001; 414:43–48. [PubMed: 11689936]
38. Shi N, Ye S, Alam A, Chen L, Jiang Y. Atomic structure of a Na^+- and K^+-conducting channel. Nature. 2006; 440:570–574. [PubMed: 16467789]
39. Kuo A, Gulbis JM, Antcliff JF, Rahman T, Lowe ED, Zimmer J, Cuthbertson J, Ashcroft FM, Ezaki T, Doyle DA. Crystal structure of the potassium channel KirBac1.1 in the closed state. Science. 2003; 300(5627):1922–1926. [PubMed: 12738871]
40. Clayton GM, Altieri S, Heginbotham L, Unger VM, Morais-Cabral JH. Structure of the transmembrane regions of a bacterial cyclic nucleotide-regulated channel. Proc Natl Acad Sci U S A. 2008; 105(5):1511–1515. [PubMed: 18216238]
41. Sali A, Blundell TL. Comparative protein modelling by satisfaction of spatial restraints. J Mol Biol. 1993; 234:779–815. [PubMed: 8254673]

42. Fiser A, Do RK, Sali A. Modeling of loops in protein structures. Protein Science. 2000; 9:1753–1773. [PubMed: 11045621]
43. Ranatunga KM, Shrivastava IH, Smith GR, Sansom MSP. Side-chain ionization states in a potassium channel. Biophys J. 2001; 80:1210–1219. [PubMed: 11222285]
44. Berneche S, Roux B. The ionization state and the conformation of Glu-71 in the KcsA K1 channel. Biophys J. 2002; 82:772–780. [PubMed: 11806919]
45. Khalili-Araghi F, Tajkhorshid E, Schulten K. Dynamics of K^+ ion conduction through Kv1.2. Biophys J. 2006; 91(6):L72–4. [PubMed: 16844753]
46. Jorgensen WL, Chandrasekhar J, Madura JD, Impey RW, Klein ML. Comparison of simple potential functions for simulating liquid water. J Chem Phys. 1983; 79:926–935.
47. Gullingsrud J, Schulten K. Lipid bilayer pressure profiles and mechanosensitive channel gating. Biophys J. 2004; 86:3496–3509. [PubMed: 15189849]
48. Kucerka N, Tristram-Nagle S, Nagle JF. Structure of fully hydrated fluid phase lipid bilayers with monounsaturated chains. J Membr Biol. 2005; 208:193–202. [PubMed: 16604469]
49. Humphrey W, Dalke A, Schulten K. VMD - Visual Molecular Dynamics. J Mol Graphics. 1996; 14:33–38.
50. Phillips JC, Braun R, Wang W, Gumbart J, Tajkhorshid E, Villa E, Chipot C, Skeel RD, Kale L, Schulten K. Scalable molecular dynamics with NAMD. J Comput Chem. 2005; 26:1781–1802. [PubMed: 16222654]
51. MacKerell AD, Bashford D, Bellott M, Dunbrack RL, Evanseck JD, Field MJ, Fischer S, Gao J, Guo H, Ha S, Joseph-McCarthy D, Kuchnir L, Kuczera K, Lau FTK, Mattos C, Michnick S, Ngo T, Nguyen DT, Prodhom B, Reiher WE, Roux B, Schlenkrich M, Smith JC, Stote R, Straub J, Watanabe M, Wiorkiewicz-Kuczera J, Yin D, Karplus M. All-atom empirical potential for molecular modeling and dynamics studies of proteins. J Phys Chem B. 1998; 102:3586–3616.
52. MacKerell AD. Empirical force fields for biological macromolecules: overview and issues. J Comput Chem. 2004; 25:1584–1606. [PubMed: 15264253]
53. Freedberg DI, Venable RM, Rossi A, Bull TE, Pastor RW. Discriminating the helical forms of peptides by NMR and molecular dynamics simulation. J Am Chem Soc. 2004; 126:10478–10484. [PubMed: 15315464]
54. Buck M, Bouguet-Bonnet S, Pastor RW, MacKerell AD Jr. Importance of the CMAP correction to the CHARMM22 protein force field: dynamics of hen lysozyme. Biophys J. 2006; 90(4):L36–38. [PubMed: 16361340]
55. Martyna GJ, Tobias DJ, Klein ML. Constant-pressure molecular-dynamics algorithms. J Chem Phys. 1994; 101:4177–4189.
56. Feller SE, Zhang YH, Pastor RW, Brooks BR. Constant-pressure molecular-dynamics simulation - the Langevin piston method. J Chem Phys. 1995; 103:4613–4621.
57. Darden T, York D, Pedersen L. Particle mesh Ewald - an N log(N) method for Ewald sums in large systems. J Chem Phys. 1993; 98:10089–10092.
58. Smart OS, Goodfellow JM, Wallace BA. The Pore Dimensions of Gramicidin A. Biophys J. 1993; 65:2455–2460. [PubMed: 7508762]
59. Frishman D, Argos P. Knowledge-based secondary structure assignment Proteins: structure, function and genetics. 1995; 23:566–579.
60. Gullingsrud J, Schulten K. Gating of MscL studied by steered molecular dynamics. Biophys J. 2003; 85(4):2087–2099. [PubMed: 14507677]
61. Lindahl E, Edholm O. Mesoscopic undulations and thickness fluctuations in lipid bilayers from molecular dynamics simulations. Biophys J. 2000; 79(1):426–433. [PubMed: 10866968]
62. Gullingsrud J, Schulten K. Lipid bilayer pressure profiles and mechanosensitive channel gating. Biophys J. 2004; 86(6):3496–3509. [PubMed: 15189849]

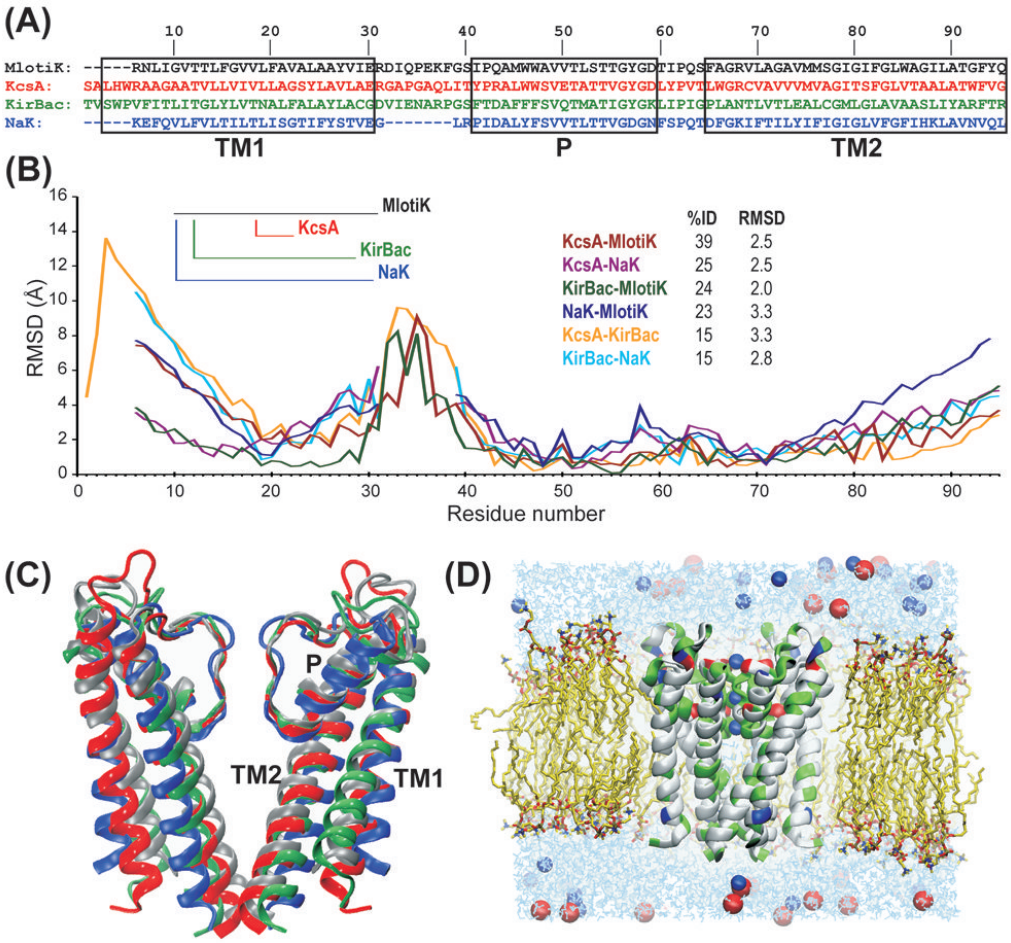

Fig. 1.

Structures used for benchmarking. (A) sequence alignment used for homology modeling, corresponding to the structural alignment. Residue numbering indicates position in the alignment. Rectangles delimit different structural regions: first transmembrane helix (TM1), P segment (P) and second transmembrane helix (TM2); (B) Deviation between the four structures as a function of residue number (the numbering scheme is maintained). The inset table indicates the percentage of sequence identity on the first column and the average RMSD (Å) between structures on the second column; (C) structure superposition of the four channels. Coloring code and structural regions are the same as in panel (A). Only two subunits are displayed for clarity; (D) sample simulation system, including the protein embedded in the lipid bilayer, water and counterions.

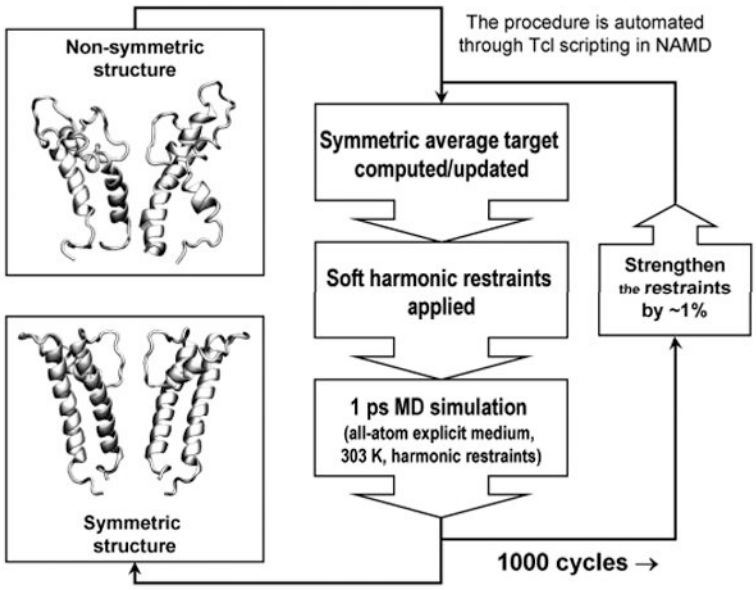

Fig. 2.
Symmetry-driven simulated annealing scheme (See Methods for details).

Fig. 3.
Simulation protocol used for all systems.

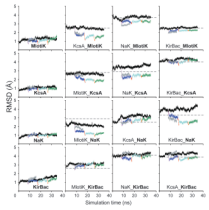

Fig. 4.

RMSD of all Cα atoms as a function of simulation time (ns), calculated using the crystal structure of the target channel as reference, for crystal structures and HMs of each protein: MlotiK (first row) KcsA (second row), NaK (third row) and KirBac (fourth row). The color scheme is the same as in Fig. 3 but only trajectories corresponding to the central and rightmost branches in Fig. 3 are displayed, for clarity. The dashed, grey lines correspond to the RMSD between the crystal structure and the initial model, before any simulation.

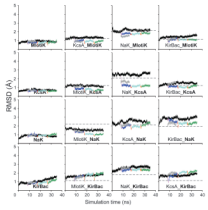

Fig. 5.

RMSD of Cα atoms of the core region (calculated using the crystal structure of the target as reference) as a function of simulation time (ns), where core is defined as: residues 163 to 210 for MlotiK, residues 63 to 110 for KcsA, residues 51 to 98 for NaK and residues 84 to 131 for KirBac. The order of the plots is the same as in Fig. 4. The color scheme is the same as in Fig. 3 but only trajectories corresponding to the rightmost branch in Fig. 3 are displayed, for clarity.

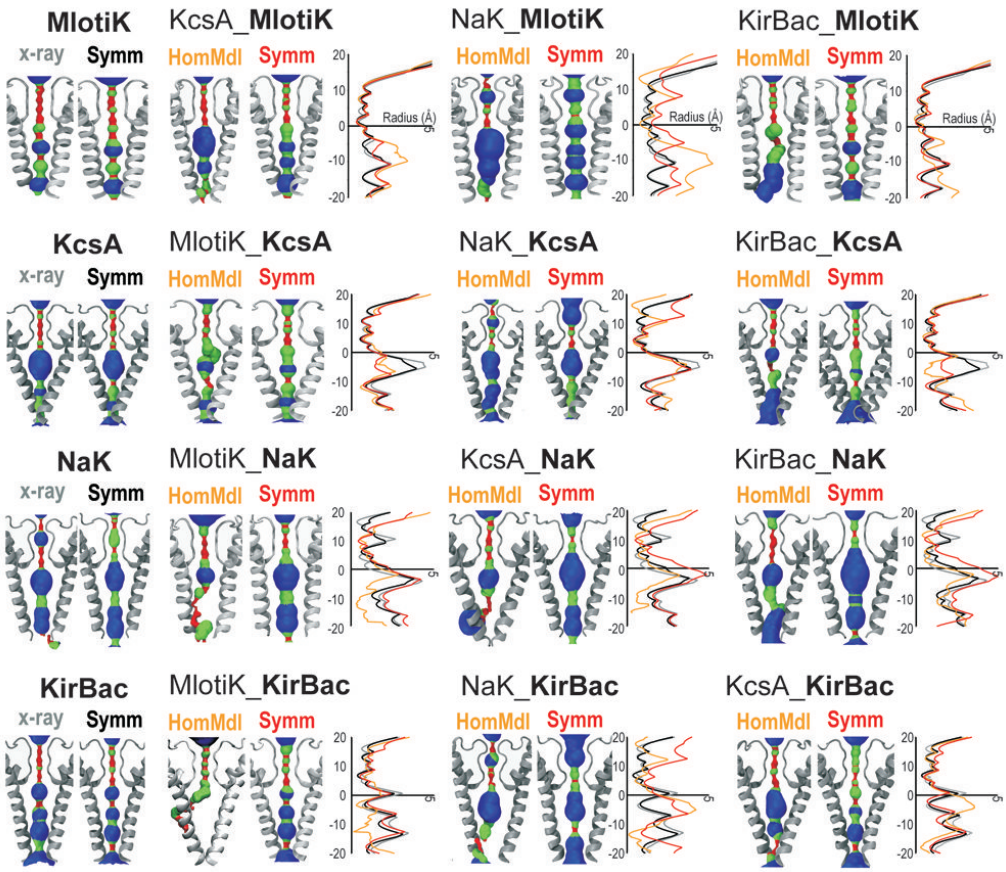

Fig. 6.

Pore shape calculated using the program HOLE, for the crystal structures and HMs (before simulation and after the second symmetry annealing). Pore regions that are inaccessible to water (pore radius < 1.15 Å) are red, water accessible parts (1.15 Å < pore radius < 2.30 Å) are green and wide areas (pore radius > 2.30 Å are blue). Plots represent pore radius as a function of z coordinate, for the crystal structure (gray), symmetricized crystal structure (black), initial homology model (orange) and symmetricized model (red).

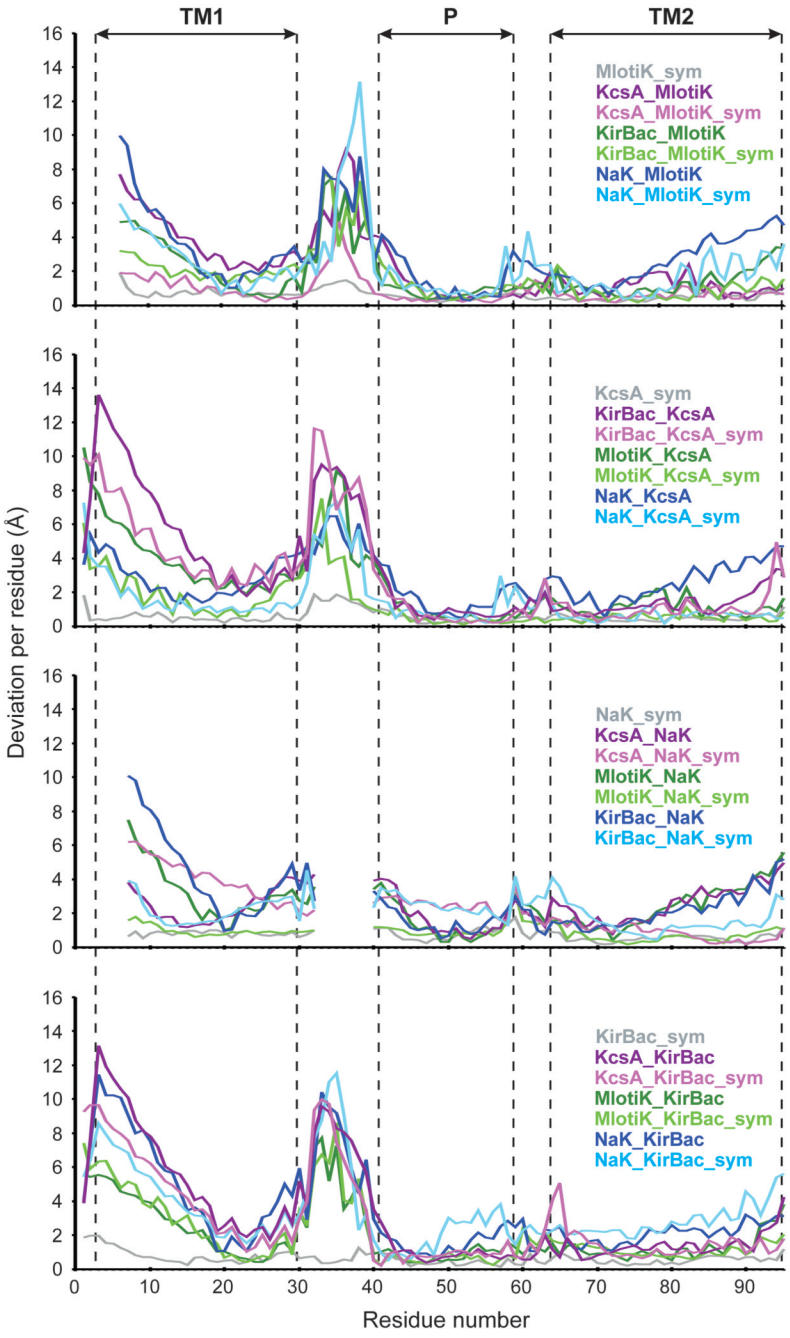

Fig. 7.

Deviation from the crystal structure of Cα atoms of each residue, calculated for the initial models, the models at the end of second annealing step and the crystal structure at the end of the second annealing step. Core trace was used for alignment.

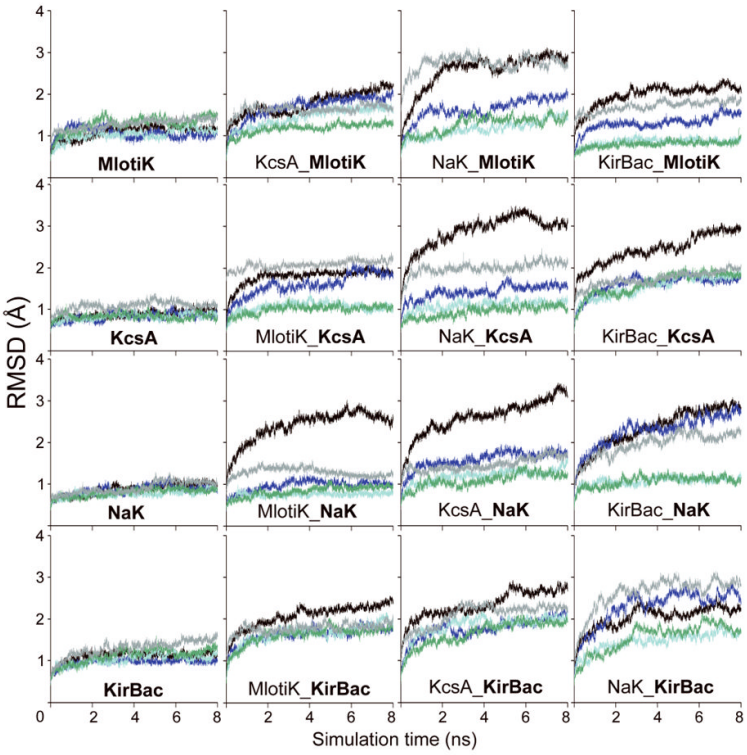

Fig. 8.

Structural stability during unrestrained simulation, calculated as RMSD of Cα atoms from the initial structure of each trajectory. Only the first 8ns of unrestrained simulation are shown (black lines). The color scheme is the same as in Fig. 3.

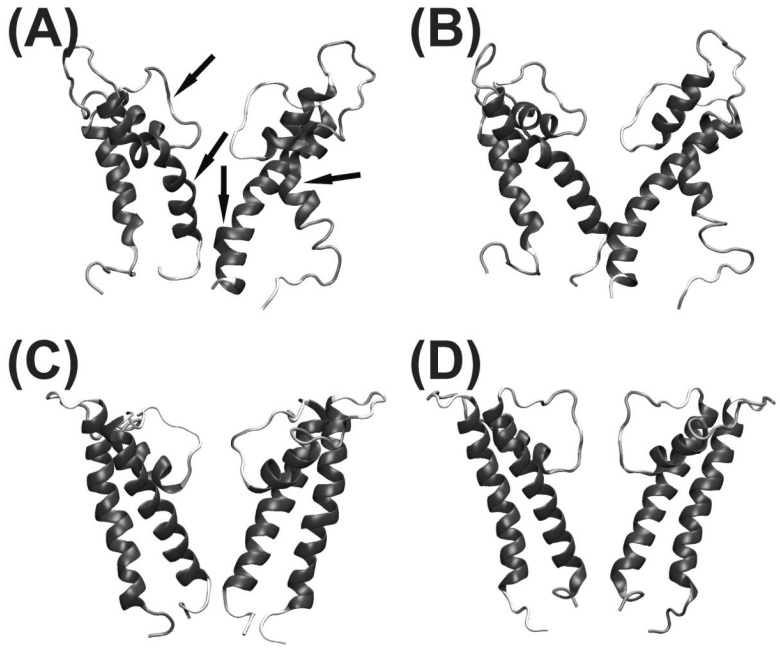

Fig. 9.

Healing of thermal defects by symmetry annealing. (A) most thermally damaged structure after 8 ns simulation at 600K without CMAP correction; (B) the structure after unrestrained simulation at 300K, with CMAP correction; (C) the structure after symmetry annealing at 600K, without CMAP correction; (D) the structure after the symmetry annealing at 300K, with CMAP correction.

Table I

Improvement in quality of homology models during particular symmetrization steps, measured as percentage of RMSD decrease against x-ray structure :

$$\Delta = 100\frac{(R_{before} - R_{after})}{R_{before}}.$$

In the MD columns, R_{before} and R_{after} are RMSDs calculated at the beginning and at the end of the particular symmetrization procedure for all the alpha-carbons (the whole channel structure was used for alignment). Note that during the unrestrained simulation steps between the symmetrizations the structures were gradually drifting away from the target, therefore the percentages of improvement presented in the table are not exactly additive. In the HM columns, R_{before} is the deviation of the initial model, before any simulation (corresponding to the dashed gray lines in Fig. 4) and R_{after} is the deviation after the particular symmetrization procedure.

	instantaneous symmetrization (first frame of the gray lines on fig. 4, 5, and 8)		**first symmetry annealing (last frame of the magenta lines)**		**second symmetry annealing (last frame of the red lines)**		**third symmetry annealing (last frame of the orange lines)**	
	MD	**HM**	**MD**	**HM**	**MD**	**HM**	**MD**	**HM**
KcsA_**MlotiK**	26.7	21.5	30.7	27.1	40.0	54.0	25.9	54.6
NaK_**MlotiK**	14.6	21.9	3.7	11.7	0.7	14.3	5.3	12.8
KirBac_**MlotiK**	22.9	25.8	16.4	19.8	6.3	11.4	2.6	9.4
MlotiK_**KcsA**	4.7	12.8	6.0	12.7	15.9	40.3	12.33	40.1
NaK_**KcsA**	25.6	13.9	31.1	31.7	6.8	29.2	8.5	21.5
KirBac_**KcsA**	3.3	-0.4	9.2	2.8	7.9	7.2	-2.3	-7.4
MlotiK_**NaK**	23.9	39.9	40.5	52.8	30.8	65.5	29.7	71.8
KcsA_**NaK**	18.5	-0.1	30.3	14.5	7.9	2.3	6.2	-9.0
KirBac_**NaK**	21.5	11.6	20.7	5.2	22.7	32.0	7.9	33.6
MlotiK_**KirBac**	21.8	10.8	18.2	5.2	11.6	-0.3	18.2	-1.8
NaK_**KirBac**	1.8	4.1	9.8	11.5	-3.9	7.7	6.9	10.6
KcsA_**KirBac**	4.7	-0.9	20.5	11.8	10.7	9.0	3.9	5.9
Average improvement		13.4		17.3		22.7		20.2

Table II

Improvement in quality of core region of homology models during particular symmetrization steps (for details see legend of Table I)

	instantaneous symmetrization (first frame of the gray lines on fig. 4, 5, and 8)		first symmetry annealing (last frame of the magenta lines)		second symmetry annealing (last frame of the red lines)		third symmetry annealing (last frame of the orange lines)	
	MD	**HM**	**MD**	**HM**	**MD**	**HM**	**MD**	**HM**
KcsA_**MlotiK**	45.5	39.4	31.3	29.6	39.1	46.1	27.5	48.2
NaK_**MlotiK**	22.0	27.2	16.4	21.8	5.0	21.7	-0.5	20.3
KirBac_**MlotiK**	35.3	18.7	35.4	18.3	26.9	13.5	1.2	-1.1
MlotiK_**KcsA**	14.2	13.2	38.0	35.2	42.3	60.1	36.5	66.9
NaK_**KcsA**	24.4	13.2	51.8	44.0	18.9	54.7	20.1	51.6
KirBac_**KcsA**	17.6	3.0	30.8	19.0	17.2	18.7	-2.3	15.6
MlotiK_**NaK**	17.8	36.7	24.9	43.9	28.3	54.7	21.0	62.0
KcsA_**NaK**	16.8	8.5	25.2	19.6	11.1	16.4	6.6	8.2
KirBac_**NaK**	28.6	-8.4	-0.5	-49.5	14.9	-15.0	6.5	-12.9
MlotiK_**KirBac**	38.2	11.4	26.8	-6.9	45.2	8.1	26.2	-23.5
NaK_**KirBac**	-0.2	-42.7	5.6	-32.6	4.6	-31.4	1.0	-25.4
KcsA_**KirBac**	24.3	-10.1	31.4	6.0	18.5	-32.9	12.3	-64.3
Average improvement		9.2		12.4		17.9		12.1